Ab Initio Molecular Orbital Calculations of the Potential Energy Surfaces for the N(^{2}D) + CH_4 Reaction

Yuzuru Kurosaki and Toshiyuki Takayanagi*

Advanced Science Research Center, Japan Atomic Energy Research Institute, Tokai-mura, Naka-gun, Ibaraki 319-11, Japan

Kei Sato and Shigeru Tsunashima

Department of Applied Physics, Faculty of Science, Tokyo Institute of Technology, Ookayama, Meguro-ku, Tokyo 152, Japan

Received: August 6, 1997; In Final Form: October 15, 1997[⊗]

Ab initio molecular orbital calculations have been carried out on the N(^{2}D) + CH_4 reaction in order to obtain information on possible reaction products. Stationary points associated with the product channels and their harmonic vibrational frequencies have been calculated at the MP2(full)/cc-pVTZ level of theory. Barrier heights and heats of reaction have been estimated at the projected MP4(full,SDTQ)/cc-pVTZ level of theory. Among the possible processes considered, the reaction pathways to produce CH_2NH + H and CH_3 + NH have been found to be important. RRKM calculations have been performed to confirm this result. The saddle point structure in the entrance channel of the N(^{2}D) + CH_4 reaction has also been calculated using the CASSCF method. It has been found that N(^{2}D) inserts into the C−H bond of CH_4, which is qualitatively consistent with recent experimental results.

Introduction

An electronically excited metastable nitrogen atom, N(^{2}D), is known to be one of the important reactive species in the various fields such as atmospheric chemistry and combustion chemistry; however, its reactivity with hydrocarbons is still unclear. There have been no reports in which the reaction products were directly identified in the reaction of N(^{2}D) with hydrocarbons, although overall rate constants for the reactions of N(^{2}D) with some hydrocarbon molecules have been measured.[1,2] Very recently, Umemoto et al.[3,4] reported the nascent rotational and vibrational distributions of NH($X\ ^3\Sigma^-$) produced in the reaction of N(^{2}D) with CH_4 using a laser-induced fluorescence technique. As far as we are aware, this is the first report in which the initial reaction product has been detected. They have compared the observed distributions of NH to those of OH($X\ ^2\Pi$) produced in the reaction of O(^{1}D) with CH_4[5−7] and found that both the distributions are very similar. Since it is generally accepted that O(^{1}D) inserts into the C−H bond of CH_4, Umemoto et al.[3,4] have suggested that N(^{2}D) also inserts into the C−H bond.

The dynamics and reaction pathways for the O(^{1}D) + CH_4 reaction have been extensively studied both experimentally and theoretically. Since the potential energy surface for the O(^{1}D) + CH_4 reaction adiabatically correlates to the stable CH_3OH structure, the primary products for this reaction are essentially the same as the products of unimolecular decomposition of CH_3-OH. It is already known that the reaction pathway to produce CH_3 + OH is the most dominant process with the branching fraction being about 0.9.[8−11] The reaction pathway to produce CH_3O + H has also been found although the branching fraction for this process has been reported to be about 0.14−0.25.[12,13] The lifetime of the CH_3OH intermediate complex has been measured to be 3 ps using the photodissociation of O_3·CH_4 complexes.[14] This "short" lifetime is consistent with the hot vibrational and rotational distributions[5−7] of OH produced in the reaction of O(^{1}D) with CH_4. On the theoretical side, possible decomposition pathways of CH_3OH have been accurately characterized using the ab initio molecular orbital (MO) method.[15,16] In addition, the potential energy surface for the O(^{1}D) + CH_4 reaction has been recently calculated by Arai et al. using the multireference single and double configuration interaction (MRSDCI) method.[17] According to their calculation, the reaction has a saddle point having a collinear O−H−C structure in the entrance region of the potential energy surface. After this saddle point O(^{1}D) moves off from the C−H axis along the minimum-energy path, and the structure approaches that of the stable CH_3OH. These results clearly demonstrate that O(^{1}D) inserts into the C−H bond. However, they have also suggested that abstraction mechanisms are also possible.

In contrast to the extensive experimental and theoretical studies for the O(^{1}D) + CH_4 reaction mentioned above, information on the detailed dynamics and reaction pathways of the N(^{2}D) + CH_4 reaction is still insufficient. As mentioned previously, only NH has been detected as a primary product,[3,4] and other reaction pathways have not been identified yet. One of the purposes of the present study is to obtain information about the possible product channels of the N(^{2}D) + CH_4 reaction theoretically. The second purpose is to understand the detailed mechanism of the reaction whether the reaction is insertive or abstractive. In the present study several stationary points on the potential energy surface for the N(^{2}D) + CH_4 reaction are characterized using ab initio MO calculations.

* Corresponding author: E-mail tako@popsvr.tokai.jaeri.go.jp.
⊗ Abstract published in *Advance ACS Abstracts,* December 1, 1997.

S1089-5639(97)02565-6 CCC: $15.00
Published on Web 01/01/1998

Computational Method

All the calculations were performed with the GAUSSIAN 94 system of programs.[18] Geometries were fully optimized at the MP2(full) level of theory using the correlation consistent polarized valence triple-ζ (cc-pVTZ) basis set of Dunning.[19] Harmonic vibrational frequencies and zero-point energies were calculated at the same level of theory. The final energy diagram was obtained from the MP4(full,SDTQ)/cc-pVTZ calculations, in which the spin projection method was applied in order to remove the spin contamination from unwanted spin states (denoted here by PMP4). This technique has previously been employed on the potential energy surface calculations for the $N(^4S,^2D) + CH_3$ reaction system.[20] Spin−orbit interactions were not taken into account in the present calculations.

The geometry at the saddle point for the $N(^2D) + CH_4$ reaction, which should exist in the entrance channel region of the potential energy surface, was optimized at the complete active space self-consistent-field (CASSCF) level of theory with the cc-pVTZ basis set since we found that use of a single reference Hartree−Fock (HF) wave function was not a good approximation. This is because the single reference HF wave function is affected by a considerable amount of spin contamination.[20] The active space employed includes five orbitals: three nitrogen *2*p orbitals, CH σ, and CH σ* orbitals of the breaking CH bond in CH_4. Five electrons were distributed among these five orbitals. The intrinsic reaction coordinate (IRC) calculations were also carried out to understand the reaction mechanism using the CASSCF level of theory but with a somewhat smaller basis set, 6-311G**, to save computational time.

Results and Discussion

A. Energy Diagram and Optimized Geometries. Figures 1 and 2 show the optimized geometries for the various stationary points on the doublet potential energy surface for the $N(^2D) + CH_4$ reaction. The geometry of CH_3N was essentially the same as that reported by Gonzalez and Schlegel[20] and is excluded in Figure 1. The harmonic vibrational frequencies for these stationary points are summarized in Table 1. The agreement between the calculated frequencies and available experimental data[21−23] is generally seen to be good, although the calculated frequencies are somewhat larger than the experimental ones. Table 2 shows the total energies at the MP2(full) and PMP4-(full,SDTQ) levels calculated with the cc-pVTZ basis set at the MP2(full)/cc-pVTZ optimized geometry as well as the zero-point energy correction (ZPE) for all the species involved in the reaction $N(^2D) + CH_4 \rightarrow$ products. The corresponding relative energies are schematically shown in Figure 3. Also included in Figure 3 are the relative energies obtained from available experimental thermochemical data.[21] It can be concluded that the relative energies of the present ab initio calculations are reliable within about 4 kcal/mol.

The structure of the saddle point (TS1) for the $N(^2D) + CH_4$ reaction is shown in Figure 2a, which was obtained at the CASSCF(5,5)/cc-pVTZ level. Essentially the same geometry was obtained with the smaller basis set, 6-311G**. The structure of the CH_4 moiety at the saddle point was almost the same as that of stable CH_4, although the distances of two of the C−H bonds were slightly larger than those of CH_4. The internuclar distance between the N atom and the nearest H atom was 1.5 Å. This means that the $N(^2D) + CH_4$ reaction is classified to have an "early" saddle point. It has been reported that the $O(^1D) + CH_4$ reaction also has an early saddle point;[17] however, the saddle point geometry for $O(^1D) + CH_4$ is different from that for $N(^2D) + CH_4$. In the case of $O(^1D) + CH_4$, the

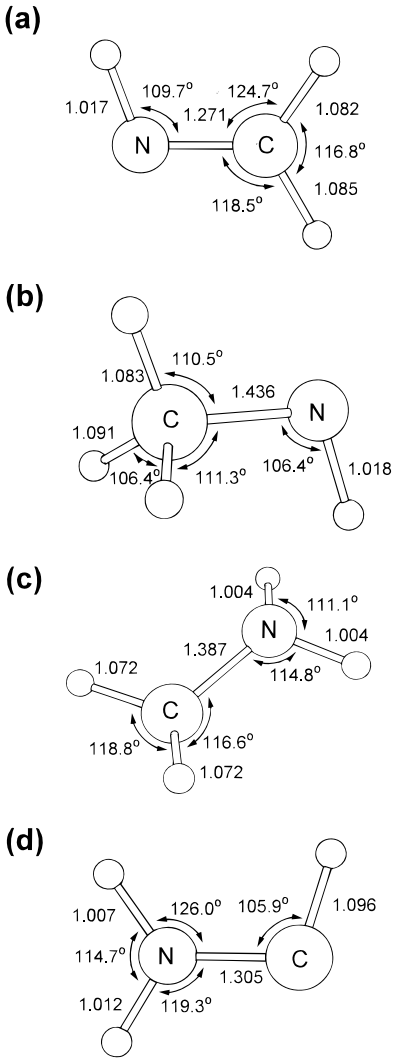

Figure 1. Geometries of the stationary points (minima) on the potential energy surface for the $N(^2D) + CH_4$ reaction: (a) CH_2NH, (b) CH_3-NH, (c) CH_2NH_2, and (d) $CHNH_2$. All the geometrical parameters were obtained at the MP2(full)/cc-pVTZ level of theory (bond lengths in angstroms, angles in degrees).

O−H−C angle was 180°,[17] while the N−H−C angle was calculated to be 123°. The barrier height including zero-point energy correction was calculated to be 5.5 kcal/mol at the PMP4-(full,SDTQ)/cc-pVTZ//CASSCF(5,5)/cc-pVTZ level of theory. Since the thermal rate constant for the $N(^2D) + CH_4$ reaction at room temperature has been reported to be about $\sim 10^{-12}$ cm^3 molecule^{-1} s^{-1}, the calculated barrier height seems to be too large. This will be discussed in detail in the following section. It is also informative to report the barrier height calculated at the CASSCF level. The calculated barrier heights was 3.0 kcal/mol at the CASSCF(5,5)/cc-pvtz level while 3.5 kcal/mol at the CASSCF(5,5)/6-311G** level. Note that the barrier height calculated at the PMP4 level is slightly larger than these CASSCF values; however, it is generally known that the CASSCF method does not include the dynamical electron correlation effect and that the PMP4 theory does not include the nondynamical electron correlation effect. The above result suggests that the nondynamical electron correlation effect is rather important for estimating the barrier height of the $N(^2D) + CH_4$ reaction. In addition, to obtain a more accurate barrier height, the MRSDCI calculation would be necessary since the MRSDCI method include both dynamical and nondynamical electron correlation effects.

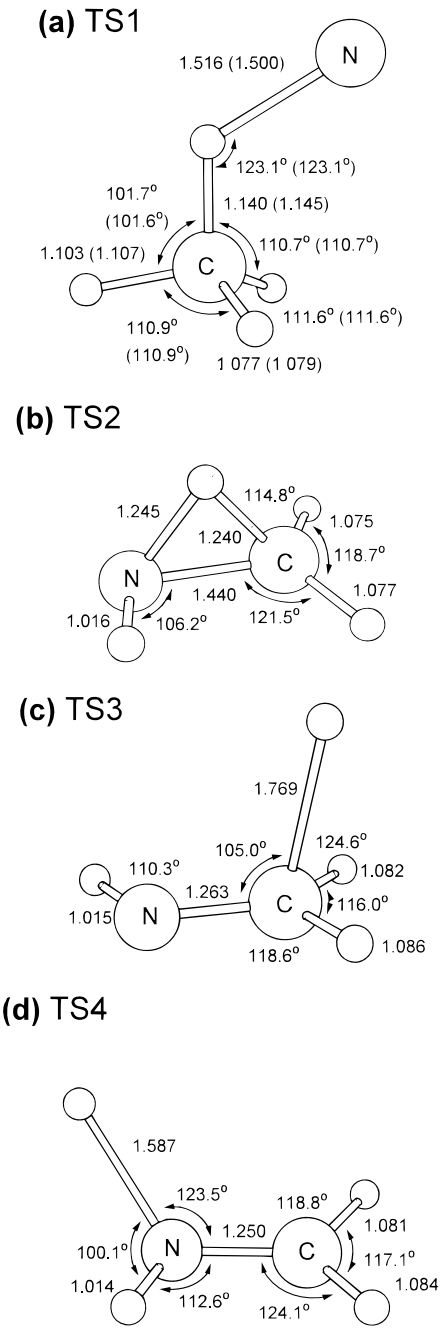

Figure 2. Geometries of the stationary points (saddle point) on the potential energy surface for the $N(^2D) + CH_4$ reaction: (a) TS1, (b) TS2, (c) TS3, and (d) TS4. The geometry for TS1 was obtained at the CASSCF(5,5)/cc-pVTZ level, while values in parentheses are the results obtained at the CASSCF(5,5)/6-311G** level. The geometries for TS2, TS3, and TS4 were obtained at the MP2(full)/cc-pVTZ level (bond lengths in angstroms, angles in degrees).

The intermediate radical, CH_3NH, is 102 kcal/mol more stable than the reactant, $N(^2D) + CH_4$. The reaction pathway to produce $CH_2NH + H$ is seen to be lowest and has an exit barrier of 5 kcal/mol compared to the energy level of the product $CH_2NH + H$ channel. The CH_3NH complex can further isomerize into a more stable CH_2NH_2 structure via the saddle point (TS2) shown in Figure 2b. The barrier height for this isomerization was calculated to be 36 kcal/mol, and the energy level of TS2 was predicted to be much smaller than that of reactant energy. The existence of this isomerization pathway is in contrast with the $O(^1D) + CH_4$ case;[15−17] only CH_3OH is an intermediate complex. There should also exist H_2 molecular elimination channels from the intermediate complexes, CH_3NH and CH_2NH_2; however, the barrier height for such a process may be expected to be very large. For example, Walch[16] calculated

TABLE 1: Harmonic Vibrational Frequencies for Minima and Transition-State Structures for the $N(^2D) + CH_4 \rightarrow$ Products Reaction[a]

molecule	frequency (cm^{-1})
	Minima
$^3CH_2$	1141 (963),[b] 3234, 3446 (3190)
CH_3	501 (606), 1450 (1396), 1450 (1396), 3201 (3005), 3372 (3161), 3372 (3161)
CH_4	1358 (1306), 1358 (1306), 1358 (1306), 1600 (1526), 1600 (1526), 3093 (2914), 3216 (3020) 3216 (3020) 3216 (3020)
NH	3415 (3282)
NH_2	1557 (1497), 3468 (3219), 3569 (3301)
$^3CH_3N$	983 (902), 983 (902), 1086 (1039), 1414 (1490), 1472 (1490), 1472 (1490), 3046 (2938), 3119 (3065), 3119 (3065)
$CHNH_2$	838, 1078, 1198, 1415, 1476, 1708, 3016, 3502, 3644
CH_2NH	1084 (1058), 1120 (1061), 1185 (1127), 1383 (1344), 1507(1452), 1694 (1638), 3111 (2914), 3201(3024), 3501 (3262)
CH_3NH	261, 971, 1021, 1082, 1354, 1425, 1517, 1520, 3045, 3093, 3176, 3497
CH_2NH_2	473, 633, 701, 953, 1257, 1347, 1521, 1668, 3233, 3335, 3611, 3721
	Transition States (Saddle Points)
$[N\cdots CH_4]$ (TS1)[c]	503i, 194, 371, 1299, 1357, 1456, 1554, 1620, 2408, 2992, 3256, 3312
[HN..H..CH_2] (TS2)	2140i, 806, 930, 1014, 1115, 1256, 1359, 1497, 2543, 3186, 3299, 3522
[$HNCH_2$..H] (TS3)	1346i, 500, 554, 1093, 1216, 1235, 1396, 1508, 1688, 3108, 3199, 3534
[CH_2NH..H] (TS4)	1803i, 409, 544, 1095, 1204, 1248, 1391, 1527, 1814, 3136, 3225, 3547

[a] All the frequencies except for TS1 were calculated at the MP2(full)/cc-pVTZ level. [b] Values in parentheses indicate experimental data taken from refs 21−23. [c] The frequencies for TS1 were calculated at the CASSCF(5,5)/cc-pVTZ level of theory.

TABLE 2: Total Energies, Zero-Point Energies, and Symmetry for the Reaction $N + CH_4 \rightarrow$ Products

	total energies (au)[a]			
species	MP2/ cc-pVTZ	PMP4/ cc-pVTZ	ZPE[b](au)	sym
$N(^4S)$	−54.506 81	−54.524 47	0.0	
$N(^2D)$	−54.443 90	−54.436 59	0.0	
CH_4	−40.428 00	−40.454 61	0.045 60	T_d
NH	−55.129 73	−55.152 32	0.007 78	
CH_3	−39.750 84	−39.776 58	0.030 41	D_{3h}
$^3CH_2$	−39.069 09	−39.091 50	0.017 82	C_{2v}
NH_2	−55.783 82	−55.807 07	0.019 58	C_{2v}
CH_2NH	−94.468 08	−94.503 69	0.040 53	C_s
$CHNH_2$	−94.406 72	−94.444 10	0.040 73	C_1
CH_3NH	−95.015 14	−95.058 44	0.050 03	C_s
CH_2NH_2	−95.030 29	−95.069 16	0.051 15	C_s
$^3CH_3N$	−94.372 46	−94.415 62	0.038 03	C_{3v}
$[N\cdots CH_4]$ (TS1)[c]	−94.829 65	−94.881 98	0.045 15[d]	C_s
[HN..H..CH_2] (TS2)	−94.954 26	−94.997 78	0.046 76	C_1
[$HNCH_2$..H] (TS3)	−94.947 40	−94.998 33	0.043 35	C_1
[CH_2NH..H] (TS4)	−94.948 45	−94.996 10	0.043 61	C_1
H	−0.499 81	−0.499 81	0.0	

[a] All the geometries except for TS1 were fully optimized at the MP2(full)/cc-pVTZ level of theory. [b] Calculated at the MP2(full)/cc-pVTZ level. [c] Geometries were optimized at the CASSCF(5,5)/cc-pVTZ level. [d] Harmonic vibrational frequencies were calculated at the CASSCF(5,5)/cc-pVTZ level.

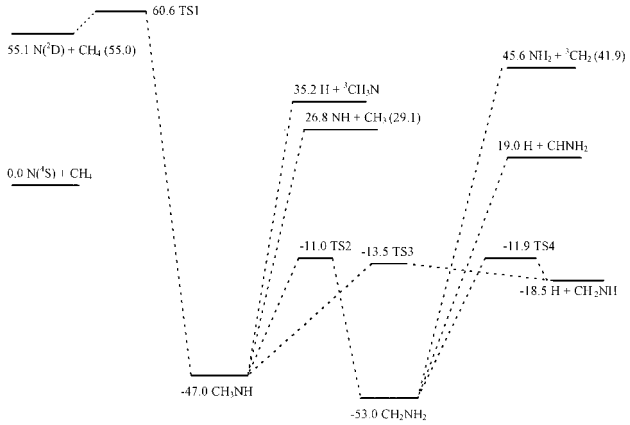

Figure 3. Calculated energy diagram (units in kcal/mol) for the $N(^2D) + CH_4 \rightarrow$ products reaction on the doublet potential surface at the PMP4(full,SDTQ)/cc-pVTZ level. Values in parentheses are taken from experimental data.[21] The energy level for the $N(^4S) + CH_4$ channel is set to be zero in this figure. TS1, TS2, TS3, and TS4 denote corresponding saddle points.

the barrier height for the $CH_3OH \rightarrow CHOH + H_2$ reaction using a high-quality ab initio MO method, which has been reported to be about 85 kcal/mol. He also reported the barrier height for $CH_3OH \rightarrow H_2CO + H_2$ to be 92 kcal/mol. If we apply these values to the H_2 elimination from CH_3NH or CH_2NH_2, the barrier height is comparable to the energy level of $N(^2D) + CH_4$. Therefore, we neglect the H_2 elimination channels from the energy diagram although such an H_2 elimination channel would be important for larger excess energy.

Consequently, the conclusion derived from the energy diagram shown in Figure 3 is that important product channels for the $N(^2D) + CH_4$ reaction are $CH_2NH + H$, $CHNH_2 + H$, and $CH_3 + NH$. This prediction will be further confirmed using RRKM calculations in the following section.

B. Reaction Mechanism for the $N(^2D) + CH_4$ Reaction. Although the saddle point geometry for the $N(^2D) + CH_4$ reaction was characterized, it is still unclear whether the reaction is insertive or not. Therefore, we have carried out IRC calculations to elucidate the reaction mechanism. An IRC trajectory is in general initiated from a saddle point toward both positive and negative directions of the eigenvector of a negative Hessian eigenvalue and is then followed stepwise along the gradient of the potential energy surface. The IRC trajectories were followed from TS1 at the CASSCF(5,5)/6-311G** level of theory with the step size being 0.05 $amu^{1/2}$ bohr. The change in geometry along IRC is plotted in Figure 4. The center of mass of the $N + CH_4$ system is fixed at the origin in the figure. The resulting IRC trajectories clearly show that $N(^2D)$ inserts into the C−H bond of CH_4. Note that the motion of the H atoms is significant since the mass-weighted coordinates are employed in the IRC calculations. In the early stage of the IRC trajectory up to the saddle point, $N(^2D)$ and CH_4 approach each other; the geometry of CH_4 in this region is essentially the same as that of the stable CH_4. After the saddle point, the C−H bond is suddenly broken while the N−H bond is newly formed at the same time. The C−N bond is gradually formed, and the structure approaches that of the stable intermediate complex, CH_3NH. The potential energy profile along IRC shown in Figure 5 also reflects this geometry change. In the region $0 < s < 2$, where s is a reaction coordinate in unit of $amu^{1/2}$ bohr, breaking of the C−H bond and formation of the N−H bond mainly occur. In the region $s > 2$, the C−N bond

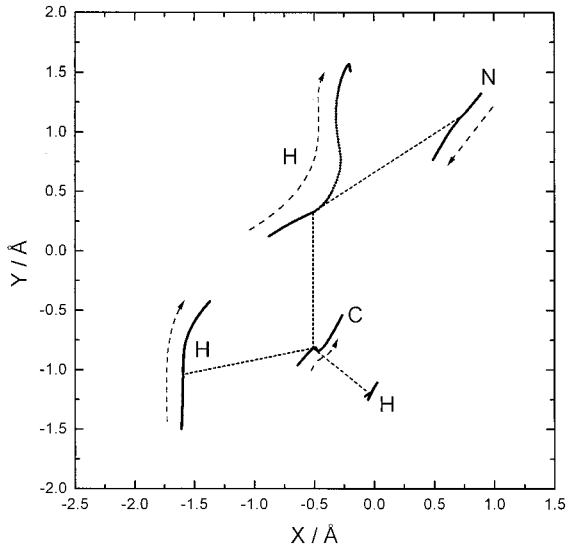

Figure 4. Geometry change along the intrinsic reaction coordinate (IRC) calculated with the CASSCF(5,5)/6-311G** level of theory. Note that the two out-of-plane H atoms are projected on the $X-Y$ plane. Arrows indicate the direction of the insertion reaction.

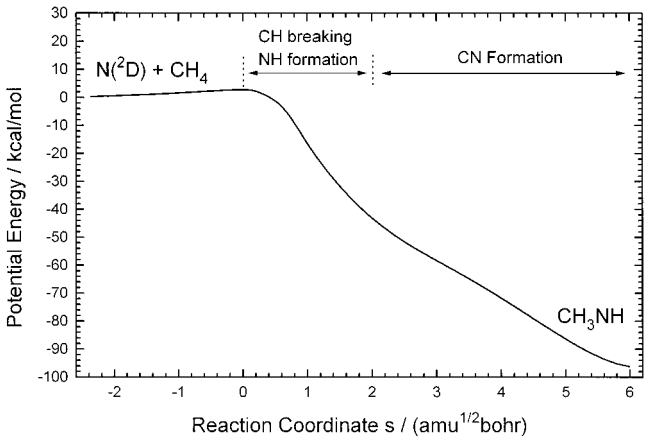

Figure 5. Potential energy profile along the intrinsic reaction coordinate calculated at the CASSCF(5,5)/6-311G** level.

is formed. This is the reason why the gradients of the potential energy in these two regions are slightly different as shown in Figure 5.

To examine the contribution of abstraction mechanism to the $N(^2D) + CH_4$ reaction further, the potential energy was calculated as a function of the N−H−C angle in Figure 6. In this figure, the internuclear distance between N and H is fixed to be 1.5 Å. Other internal coordinates were optimized. The calculations were carried out at the CASSCF(5,5)/6-311G** level of theory. It is found that the barrier height for the collinear approach of $N(^2D)$ toward the C−H bond in CH_4 is about 2 kcal/mol larger than that for the most favorable approach. Therefore, the potential energy surface calculated at the CASSCF(5,5)/6-311G** level allows only insertion mechanism at relatively low collision energies. However, a more accurate treatment of electron correlation such as MRSDCI would be necessary to obtain more quantitative results.

C. Transition-State Theory Calculations of Thermal Rate Constants. As mentioned previously, the experimental thermal rate constant[1,2] at room temperature for the $N(^2D) + CH_4$ reaction has been reported to be 3.0×10^{-12} and 4.6×10^{-12} cm^3 $molecule^{-1}$ s^{-1}. We theoretically calculated the rate constants using information obtained from the present ab initio calculations. The rate constant, *k(T)*, was calculated by

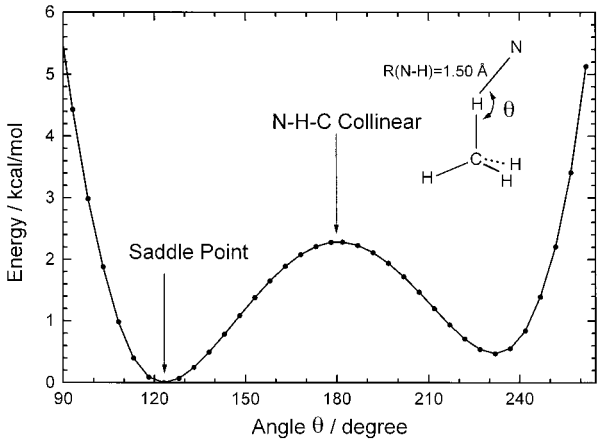

Figure 6. Potential energy as a function of the C−H−N bending angle calculated at the CASSCF(5,5)/6-311G** level. The N−H internuclear distance is fixed to be 1.5 Å. Other internal coordinates are optimized. The geometries were constrained within C_s symmetry.

conventional transition-state theory using the usual expression

$$k(T) = L\frac{k_B T}{h}\frac{Q}{Q_N Q_{CH_4}} e^{-E_0/k_B T}$$

where L is a statistical factor and is 4 in this reaction system. All the partition functions, Q's, were calculated using the ab initio vibrational frequencies shown in Table 1 and moments of inertia. If we use the ab initio value of 5.5 kcal/mol calculated at the PMP4(full,SDTQ)/cc-pVTZ//CASSCF(5,5)/cc-pVTZ level as the barrier height, E_0, the rate constant at 300 K is estimated to be 6.1×10^{-16} cm^3 molecule^{-1} s^{-1}, which is much smaller than the experimental values by a factor of about 10^4. Since it is generally known that quantum mechanical tunneling significantly increase the rate constants, we have estimated the contribution of tunneling using both the simple Wigner tunneling correction[24] and the Eckart potential.[24] As a result, the Wigner method increases the rate constant at 300 K by a factor of 1.2, while the tunneling factor calculated by the Eckart method was 1.3. These results imply that the effect of tunneling is not so important and that the ab initio barrier height of 5.5 kcal/mol is too large to obtain reasonable agreement with the experimental data. When we employ 3.0 kcal/mol as the barrier height, which corresponds to the CASSCF(5,5)/cc-pVTZ value, the rate constant at 300 K was estimated to be 4.0×10^{-14}, which is still smaller than the experimental values by a factor of 10^2. Finally, if we reduce the barrier height into 0.5 kcal/mol, the rate constant was calculated to be 3.2×10^{-12} at 300 K. Therefore, it is suggested that the insertion barrier height for the N(^{2}D) + CH_4 reaction is less than 1 kcal/mol. To further discuss the validity of this estimated barrier height, a measurement of temperature dependence of the thermal rate constants is necessary. Such an experimental work is currently underway in our laboratory.

D. RRKM Calculations of Product Branching Fractions. If the N(^{2}D) + CH_4 reaction proceeds mainly via the insertion mechanism, the product branching fractions can be determined by the unimolecular dissociation rate constants of the intermediate complexes, CH_3NH and CH_2NH_2. We have calculated the product branching fractions using the RRKM theory since such information would be important for future experimental work. The unimolecular dissociation mechanism of the intermediate complexes may be written as follows:

$$CH_3NH \xrightarrow{k_1} CH_2NH + H \quad (1)$$

$$\xrightarrow{k_2} CH_3 + NH \quad (2)$$

$$\xrightarrow{k_3} {}^3CH_3N + H \quad (3)$$

$$CH_3NH \xleftrightarrow{k_4,k_{-4}} CH_2NH_2 \quad (4)$$

$$CH_2NH_2 \xrightarrow{k_5} CHNH_2 + H \quad (5)$$

$$\xrightarrow{k_6} NH_2 + {}^3CH_2 \quad (6)$$

$$\xrightarrow{k_7} CH_2NH + H \quad (7)$$

where k_i is the corresponding unimolecular rate constant of reaction i. The unimolecular rate constants for reactions 1, 4, and 7 were calculated by standard RRKM theory using the vibrational frequencies at the MP2(full)/cc-pVTZ level of theory shown in Table 1 as well as the energetics in Table 2 since the corresponding saddle points have been found. Total energy was assumed to be the difference between the energy of TS1 and that of the reactant N(^{2}D) + CH_4 in all the RRKM calculations. The Whitten−Rabinovich approximation was used to calculate the sum of states for saddle points and density of states for the reactant molecules.

Since no saddle point was assigned for reactions 2, 3, 5, and 6 in the present ab initio calculations, these reactions can be classified as simple bond ruptures with "loose transition state". To estimate the unimolecular rate constants for these reactions, we employed a "loose transition state" model.[25] In this model the rate constants are determined by locating the position of the minimum sum of states along the reaction coordinate; i.e., reaction coordinate can be assigned as the bond distance to be broken for the simple bond rupture. The potential energy along with the rupturing bond, r, was represented by the Morse function. The parameters for the Morse function including the dissociation energy D_e, the equilibrium internuclear distance r_e, and the parameter β were determined from the present ab initio results. The variation of the vibrational frequencies along r was represented as follows:[24]

$$\nu(r) = \nu_e \exp[-\alpha(r - r_e)] + \nu_\infty\{1 - \exp[-\alpha(r - r_e)]\} \quad (8)$$

where ν_e and ν_∞ are the reactant frequency and the corresponding product frequency, respectively. For the vibrational modes that disappear in the product channel, ν_∞ was set to be zero. α is an adjustable parameter known as a "looseness parameter"[24] and mostly determines the position of the minimum sum of states. For a given parameter α, the RRKM rate constant was calculated as a function of r and the minimum value was found. The unimolecular rate constants thus calculated are summarized in Table 3. In the present study the ratio α/β was varied from 0.2 to 0.4. Note that the rate constants for reactions 2, 3, 5, and 6 increase with an increase in the value of α/β. This is because the increase in the values of α/β results in the smaller vibrational frequencies so that the increase in the state densities makes the RRKM rate constant larger.

To estimate the product branching fractions, the kinetic equations for reactions 1−7 were numerically solved with an

TABLE 3: Calculated RRKM Unimolecular Rate Constants (in units of s^{-1})

α/β[a]	k_1	k_2	k_3	k_4	k_{-4}	k_5	k_6	k_7
0.40	6.0(12)[b]	3.9(13)	5.6(11)	1.6(12)	6.0(11)	3.6(12)	3.5(13)	1.0(12)
0.35	6.0(12)	1.3(13)	3.0(11)	1.6(12)	6.0(11)	2.0(12)	5.2(12)	1.0(12)
0.30	6.0(12)	4.3(12)	1.6(11)	1.6(12)	6.0(11)	1.1(12)	7.7(11)	1.0(12)
0.25	6.0(12)	1.4(12)	8.2(10)	1.6(12)	6.0(11)	6.0(11)	1.1(11)	1.0(12)
0.20	6.0(12)	4.6(11)	4.3(10)	1.6(12)	6.0(11)	3.4(11)	1.7(11)	1.0(12)

[a] Values of β used are 2.1, 2.5, 2.9, and 2.7 in unit of $Å^{-1}$ for reactions 2, 3, 5, and 6, respectively. [b] Numbers in parentheses are multiplicative powers of 10.

TABLE 4: Calculated Product Branching Fractions

	reaction					
α/β	1	2	3	5	6	7
0.40	0.13	0.83	0.01	0.01	0.03	0.00
0.35	0.29	0.62	0.01	0.03	0.04	0.01
0.30	0.51	0.37	0.01	0.06	0.02	0.03
0.25	0.69	0.16	0.01	0.07	0.01	0.06
0.20	0.78	0.06	0.01	0.06	0.00	0.09

initial relative concentration of CH_3NH being unity. The resulting product branching fractions are summarized in Table 4 as a function of the ratio α/β. It is seen that the dominant product channels are $CH_2NH + H$ and $CH_3 + NH$ for all the values of α/β considered. Also, the branching fractions for these channels are strongly dependent on α/β since the RRKM rate constant to produce $CH_3 + NH$ strongly depends on the value of α/β as mentioned above. On the other hand, the branching fractions for reactions 5, 6, and 7 are relatively small despite that the rate constants for these reactions are dependent on the value of α/β. This is because the rate constant for the isomerization reaction 4 is smaller than that for reaction 1 or 2; i.e., reactions (1) and 2 proceed prior to the isomerization reaction.

To obtain further information on the absolute value of α/β, we have estimated this value as follows. First, the geometry optimization was done with the rupturing bond length being fixed to be $r_e + 0.3$ Å. Next, the vibrational frequencies were calculated from the projected force constant matrix[26] at this optimized geometry. The value of α for each vibrational frequency was then determined from eq 8. Although the values of α were somewhat scattered, the averaged value of α thus determined was 0.5−0.9. Therefore, the value of α/β is approximately in the range 0.24−0.31, suggesting that the contributions of both reactions 1 and 2 are important. However, we have to emphasize that the estimated value of α/β is only qualitative. To obtain more quantitative data, extensive force constant calculations along the reaction coordinate may be necessary although such calculations are very time-consuming.

Very recently, Umemoto et al.[27] have suggested that the signal intensity of $NH(v=0)$ is comparable between the $N(^2D) + CH_4$ and $N(^2D) + H_2$ reactions. This means that $CH_3 + NH$ is one of the dominant product channels in the $N(^2D) + CH_4$ reaction. Their experimental result can be qualitatively explained by the present RRKM results although a more quantitative treatment for calculating the unimolecular rate constants such as classical trajectory calculations would be needed to take the dynamical effect into account. Nevertheless, it should be emphasized that the $N(^2D) + CH_4$ reaction proceeds mainly via the insertion−dissociation mechanism and that the dominant product channels are $CH_3 + NH$ and $CH_2NH + H$.

Conclusions

Ab initio MO calculations have been carried out to study the possible product channels in the reaction of $N(^2D)$ with CH_4. Among the possible processes considered, the reaction pathways to produce $CH_2NH + H$ and $CH_3 + NH$ are important. This prediction has been further confirmed using RRKM calculations of product branching fractions. IRC calculations have also been performed to understand the detailed mechanism of the $N(^2D) + CH_4$ reaction. It has been found that $N(^2D)$ inserts into the C−H bond in CH_4 to produce the intermediate radical, CH_3NH. This result is qualitatively consistent with recent experimental results by Umemoto et al.[3,4] Further experimental studies such as a measurement of product branching fractions as well as direct detection of the reaction products would be necessary to confirm the present theoretical results. Also, on the theoretical side, classical trajectory calculations will be important to fully characterize the reaction dynamics of the $N(^2D) + CH_4$ reaction.

Acknowledgment. The authors thank Prof. Umemoto for helpful discussions.

References and Notes

(1) Schofield, K. *J. Phys. Chem. Ref. Data* **1979**, *8*, 723.
(2) Fell, B.; Rivas, I. V.; McFadden, D. L. *J. Phys. Chem*. **1981**, *85*, 224.
(3) Umemoto, H.; Kimura, Y.; Asai, T. *Chem. Phys. Lett*. **1997**, *264*, 215.
(4) Umemoto, H.; Kimura, Y.; Asai, T. *Bull. Chem. Soc. Jpn*., in press.
(5) Luntz, A. C. *J. Chem. Phys*. **1980**, *73*, 1143.
(6) Cheskis, S. G.; Iogansen, A. A.; Kirakov, P. V.; Razuvaev, I. Yu.; Sarkisov, O. M.; Titov, A. A. *Chem. Phys. Lett*. **1989**, *155*, 37.
(7) Park, C. R.; Wisenfeld, J. R. *J. Chem. Phys*. **1991**, *95*, 8166.
(8) Lin, C. L.; DeMore, W. B. *J. Phys. Chem*. **1973**, *37*, 863.
(9) Greenberg, R. I.; Heicklen, J. *Int. J. Chem. Kinet*. **1972**, *4*, 417.
(10) Jayanty, R. K. M.; Simonaitis, R.; Heicklen, J. *Int. J. Chem. Kinet*. **1976**, *8*, 107.
(11) Hack, W.; Thiesemann, H. *J. Phys. Chem*. **1995**, *99*, 17364.
(12) Satyapal, S.; Park, J.; Bersohn, R. *J. Chem. Phys*. **1989**, *91*, 6873.
(13) Matsumi, Y.; Tonokura, K.; Inagaki, Y.; Kawasaki, M. *J. Phys. Chem*. **1993**, *97*, 6816.
(14) van Zee, R. D.; Shephenson, J. C. *J. Chem. Phys*. **1995**, *102*, 6946.
(15) Harding, H. B.; Schlegel, H. B.; Krishnan, R.; Pople, J. A. *J. Phys. Chem*. **1980**, *84*, 3394.
(16) Walch, S. P. *J. Chem. Phys*. **1993**, *98*, 3136.
(17) Asai, H.; Kato, S.; Koda, S. *J. Phys. Chem*. **1994**, *98*, 12.
(18) Frisch, M. J.; Trucks, G. W.; Schlegel, H. B.; Gill, P. M. W.; Johnson, B. G.; Robb, M. A.; Cheeseman, J. R.; Keith, T.; Petersson, G. A.; Montgomery, J. A.; Raghavachari, K.; Al-Laham, M. A.; Zakrzewski, V. G.; Ortiz, J. V.; Foresman, J. B.; Cioslowski, J.; Stefanov, B. B.; Nanayakkara, A.; Challacombe, M. C.; Peng, Y.; Ayala, P. Y.; Chen, W.; Wong, M. W.; Andres, J. L.; Replogle, E. S.; Gomperts, R.; Martin, R. L.; Fox, D. J.; Binkley, J. S.; Defrees, D. J.; Baker, J.; Stewart, J. P.; Head-Gordon, M.; Gonzalez, C.; Pople, J. A. *Gaussian 94*; Gaussian, Inc.: Pittsburgh, PA, 1995.
(19) Dunning, T. H., Jr. *J. Chem. Phys*. **1989**, *90*, 1007.
(20) Gonzalez, C.; Schlegel, H. B. *J. Am. Chem. Soc*. **1992**, *114*, 9118.
(21) *JANAF Thermochemical Tables*, 3rd ed.; Natl. Stand. Ref. Data Ser. (U. S., Natl. Bur. Stand.); U.S. GPO: Washington, DC, 1985.
(22) Jacox, M. E. *J. Phys. Chem. Ref. Data* **1988**, *17*, 269.
(23) Jacox, M. E. *J. Phys. Chem. Ref. Data* **1990**, *19*, 1387.
(24) Johnston, H. S. *Gas-Phase Reaction Rate Theory*; Ronald Press: New York, 1966.
(25) Holbrook, A.; Pilling, M. J.; Robertson, S. H. *Unimolecular Reactions*; John Wiley: Chichester, 1996.
(26) Miller, W. H.; Handy, N. C.; Adams, J. E. *J. Chem. Phys*. **1980**, *72*, 99.
(27) Umemoto, H.; Kimura, Y. Private communication.